1 # Supplementary Information

2

3 # GaN-coated III–V photoelectrocatalyst with oxide-free
4 interface and ambipolar charge transport

5 *Haoqing Su[1,2], Sahar Shekarabi[3], Xiaohan Ma[1,2], Wentao Zhang[1,2], Mohammad Amin Zare Pour[3,4], Steffen*
6 *Fengler[5], Chengxing He[1,2], Tianshuo Zhao[1,2], Thomas Dittrich[5], Thomas Hannappel[3*], Shu Hu[1,2*]*

7 [1] Department of Chemical and Environmental Engineering, Yale University, New Haven, CT 06510, USA
8 [2] Energy Sciences Institute, Yale University, 810 West Campus Drive, West Haven, CT 06516, USA
9 [3] Fundamentals of Energy Materials, Institute of Physics, Technische Universität Ilmenau, 98693 Ilmenau,
10 Germany
11 [4] BMFTR Junior Research Group PARASOL, Institute of Physics, Faculty of Mathematics and Natural
12 Sciences, Technische Universität Ilmenau, 98693 Ilmenau, Germany
13 [5] Helmholtz-Zentrum Berlin für Materialien und Energie GmbH, CE-NSLI, Schwarzschildstr. 8, D-12489
14 Berlin, Germany
15 ***Corresponding Authors***

16 *E-mail: shu.hu@yale.edu, thomas.hannappel@tu-ilmenau.de*

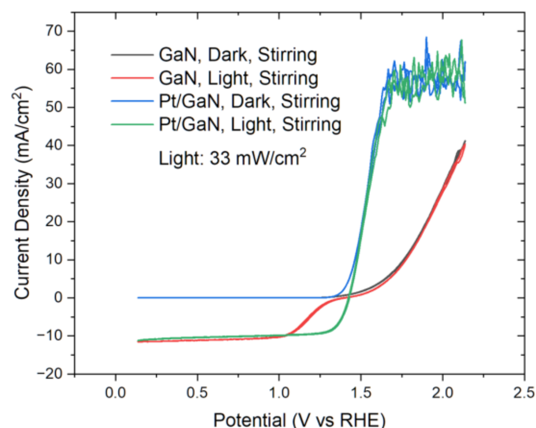

17

18 **Supplementary Fig. 1** Cyclic voltammetry of p-type InP with 10 nm GaN, with or without 2.5 nm sputtered
19 Pt, in 0.1 M K_2SO_4 electrolyte dissolved with 10 mM/10 mM ferrocyanide/ferricyanide redox mediators,
20 with the solution stirred, measured under AM 1.5G illumination (Xe lamp, 33 mW cm^{-2}) or in the dark.

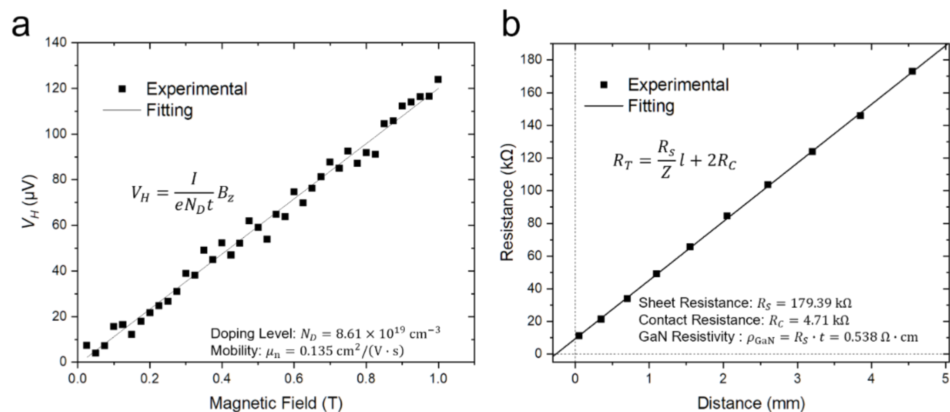

21

22 **Supplementary Fig. 2 a,** Hall measurement result and **b,** transfer length measurement (TLM) result of
23 ALD-grown 50 nm GaN on a quartz substrate. The doping level and resistivity of GaN are extracted,
24 respectively, from the measurements.

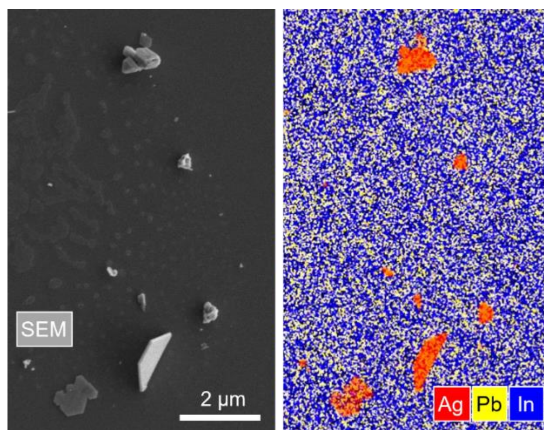

25

26 **Supplementary Fig. 3** SEM-EDX mapping of p-type InP with 10 nm TiO_2 after photoelectrochemical
27 deposition in a 10 mM $AgNO_3$ and 10 mM $Pb(NO_3)_2$ solution, both dissolved in 1M $HClO_4$ electrolytes.

28

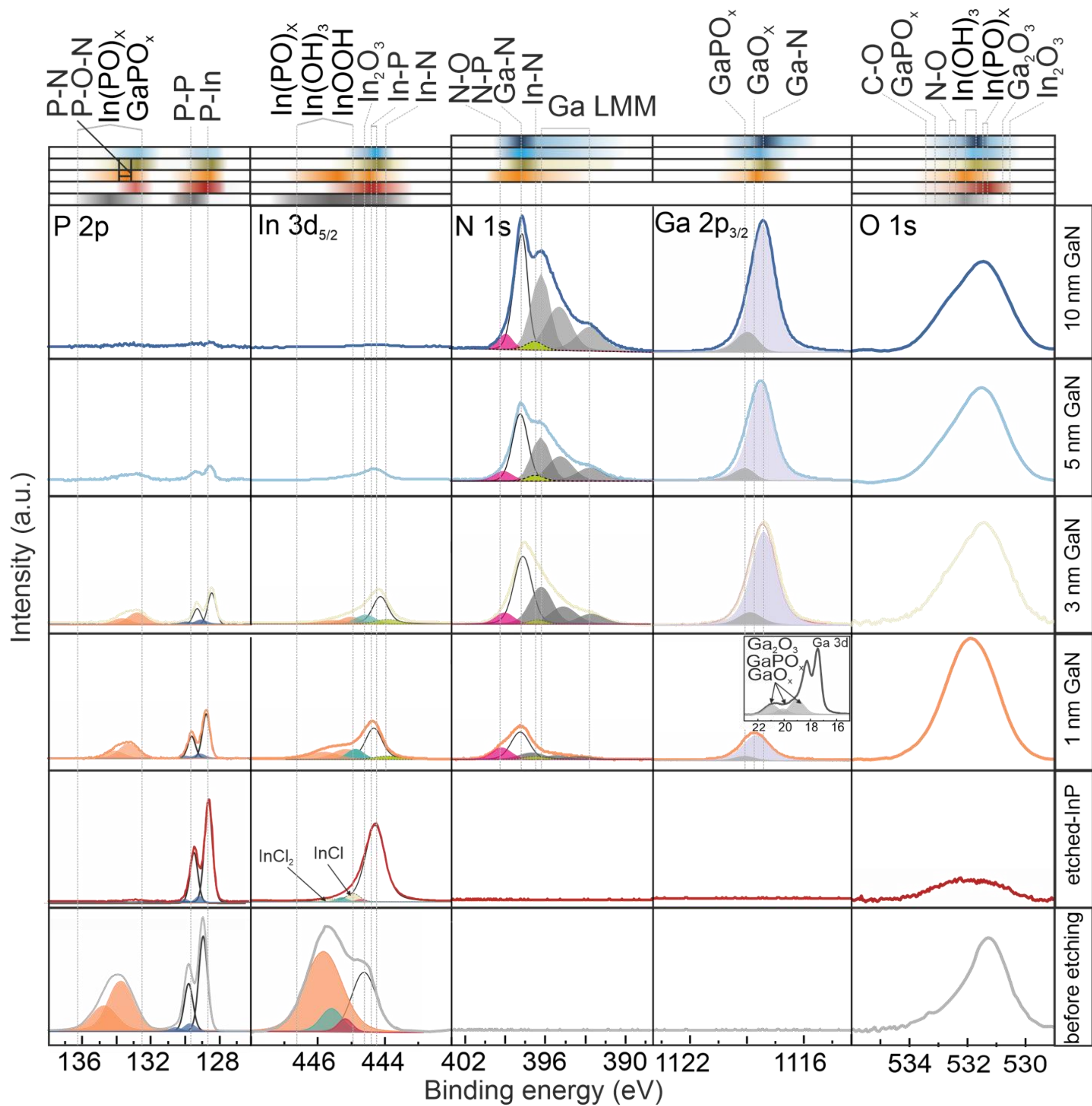

29

30 **Supplementary Fig. 4** Core-level XPS deconvolution results of P-2p, In-3d5/2, N-1s, Ga-2p3/2, and O-1s
31 region on InP samples with different thicknesses of GaN, native InP surface before etching, and InP surface
32 loaded in XPS immediately after 1 M HCl etching.

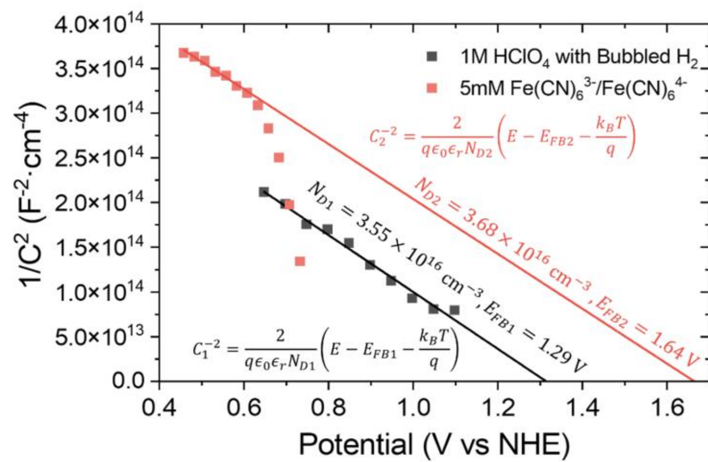

33

34 **Supplementary Fig. 5** Mott–Schottky plots of Pt/GaN/p-InP samples in the dark, measured in 1 M $HClO_4$
35 electrolytes bubbled with H_2 (black square) andin 0.1 M K_2SO_4 electrolyte dissolved with 5 mM/5 mM
36 ferrocyanide/ferricyanide redox mediators.

37

38 **Supplementary Table 1** Summary of reported performance of InP solar cell photocathodes with strategies
39 including nano/microstructure fabrications, ALD coating passivation, and chemical etching pretreatment.
40 This table shows our record-level photovoltage and photocurrent achieved by the new interface design.

Structure	**Onset potential**	**Photocurrent density** (under 1 sun)	**Stability**	**Method**	**Ref**
Single p-n junction InP solar cells	0.94 V (open circuit potential)	34 mA cm^{-2}	–	Solid-state p-n junction	US Patent 9, 590, 131 B2, 7 March 2017
pn^{+}-InP/TiO_2/Pt (InP nanopillar)	0.85 V vs RHE	28 mA cm^{-2}	6 hours	Epitaxy grown p-n^{+} junction, 4 nm TiO_2 ALD coating	Adv. Funct. Mater. 2017, 26, 679
p-InP/TiO_2/Ru (InP nanopillar)	0.73 V vs RHE	37 mA cm^{-2}	6 hours	InP nanopillars made by RIE, 5 nm TiO_2 ALD coating	Angew. Chem. Int. Ed. 2012, 51, 10760
p-InP/Pt	0.71 V vs RHE	18 mA cm^{-2}	285 hours (corroded afterward)	InP etched by Br_2 and NH_3	Energy Environ. Sci. 2021, 14, 6007
This work	0.79 V vs RHE	34 mA cm^{-2}	160 hours (no corrosion)	InP etched by HCl, 10 nm GaN ALD coating	–

41

Supplementary Table 2 Measured core level binding energies and valence band maxima (VBM) for bulk InP and GaN layers, as well as InP/GaN heterostructures with different GaN thicknesses. The calculated valence band offsets (VBO) were obtained using the Kraut method.

Samples	Peak position and VBM (eV)		VBO (eV)
Bulk InP	E VBM	0.8	–
	P 2p	128.5	
	In 3d5/2	444.3	
InP/GaN(10 nm)	E VBM	2.8	
	Ga 2p3/2	1118.1	
	N 1s	397.7	
InP/GaN(1 nm)	P 2p	128.6	2.4
	In 3d5/2	444.4	2.1
	N 1s	397.8	2.4
	Ga 2p3/2	1118.6	2.0
InP/GaN(3 nm)	P 2p	128.4	2.1
	In 3d5/2	444.2	1.9
	N 1s	397.5	2.1
	Ga 2p3/2	1118.2	1.9
InP/GaN(5 nm)	P 2p	128.6	2.1
	In 3d5/2	444.3	2.1
	N 1s	397.8	2.1
	Ga 2p3/2	1118.3	2.0

Supplementary Note 1 | Comparison of GaN and TiO_2 for photocatalysis using InP light absorber.

As shown in **Fig. 3a**, the TiO_2/InP photocathode exhibited no discernible anodic current in cyclic voltammetry under illumination in the benzoquinone/hydroquinone (50/50 mM) redox mediator, in stark contrast to the mass-transport-limited pattern observed for GaN/InP under identical conditions. Furthermore, the resulting photocatalyst exhibited a hydrogen production rate of 16.7 μmol cm^{-2} h^{-1}, whereas Rh–CrO_x/TiO_2/InP photocatalysts displayed negligible hydrogen evolution activity under identical conditions. Two factors account for the absence of ambipolar conductivity on TiO_2. First, the conduction-band offset between TiO_2 and InP (~0.45 eV) presents a large barrier for hole transfer to the surface[1,2]. This offset favors electron extraction, which underlies its utility as a photocathode protection layer. However, the same offset poses a significant barrier to hole transfer and drives oxidative reactions at the solid–liquid interface, thereby preventing TiO_2 from supporting hole transport. Second, interfacial defect states at TiO_2/InP enhance hole trapping and recombination, leaving only a negligible fraction of photogenerated holes available for interfacial reactions (as discussed in detail in the following section). Although defect states in TiO_2 coating have been proposed to mediate hole transport via intermediate-band conduction, this mechanism requires favorable energetic alignment with the InP valence band maximum[3]. In this system, the intermediate band of TiO_2 lies more positively in electrochemical potentials than the valence band maximum of InP, preventing effective hole transfer. In contrast, GaN functions not only as an effective passivation layer that promotes efficient electron conduction but also as an ambipolar coating that transports both charge-carrier types.

Supplementary Note 2 | TR-SPV signatures of residual interfacial states and Pt-induced charge-carrier separation at GaN/InP interfaces.

In addition to quantifying defect density, energy-resolved TR-SPV also reveals energetic features relevant to charge-carrier separation across the GaN-coated interface under photocatalytic conditions. Because the ambipolar transport discussed above may be associated with the remaining shallow interfacial states, we next analyze the absolute SPV spectra extracted at fixed delay times (**Fig. 4b**) to determine the energetic distribution of the residual interfacial states and the relaxation kinetics of the SPV response they support, thereby distinguishing shallow states compatible with charge-carrier transfer. In this analysis, the energetic position of the SPV features distinguishes between deeper and shallower defect states, whereas their time evolution indicates which states remain long-lived and which decay rapidly. At 10 ns after the laser pulse, the maximum positive SPV signals appeared at ~1.25 eV and reached 0.17 and 0.10 V for samples #1 (TiO_2/InP) and #2 (Pt/TiO_2/InP), respectively. For sample #3 (GaN/InP), the maximum positive SPV signal was only about 3 mV, and for sample #4 (Pt/GaN/InP) no positive signal was detected above the noise level (~0.3 mV at 1.2 eV). Thus, even at the earliest delay time, the population of promptly active deep states is already drastically suppressed at GaN/InP relative to TiO_2/InP and is further reduced by the Pt overlayer by about 1.7-fold on TiO_2/InP and about tenfold on GaN/InP. At longer delay times, the spectra further distinguish the nature of the remaining states. After 10 ms, a shoulder of

86 positive SPV signal appears at ~1.1 eV for all samples, indicating the presence of relatively shallow
87 traps at the InP surface. For sample #1 (TiO_2/InP), the negative SPV signals also increase near the
88 absorption onset of TiO_2 (~3.3 eV), and the SPV signals excited above 3.3 eV decay more slowly
89 than those excited below 3.3 eV. By contrast, SPV signals related to fundamental absorption in
90 TiO_2 are not observed on samples #2 (Pt/ TiO_2/InP), #3 (GaN/InP), or #4 (Pt/GaN/InP). As a high-
91 work-function metal (~5.6 eV), a Pt overlayer establishes a strongly coupled electron sink at the
92 GaN surface and effectively pins the surface Fermi level, so electrons are preferentially transferred
93 into Pt rather than stored in GaN/InP-related defect states. This band-alignment picture explains
94 the additional reduction of N_{Q+} from ~10^{10} cm^{-2} for GaN/InP to below ~10^{9} cm^{-2} for Pt/GaN/InP.
95 On Pt/ TiO_2/InP, Pt acts as a recombination contact for charge carriers photogenerated in the TiO_2
96 surface layer, preventing this excitation channel from producing additional SPV. On Pt/GaN/InP,
97 Pt instead acts primarily as an efficient sink for electrons transferred from InP through the GaN
98 layer, which increases the average charge-carrier-separation length and therefore enhances the
99 negative SPV signal relative to GaN/InP without Pt. In a photocatalytic configuration, where Pt-
100 covered regions act as electron-collecting reduction sites while adjacent uncovered GaN regions
101 remain available for hole transfer, this interfacial asymmetry can further establish a lateral driving
102 force for charge-carrier separation. Therefore, the residual interfacial states at GaN/InP are shallow
103 enough to remain compatible with hole transfer across the coating, as required by the ambipolar
104 PEC and photocatalytic responses in **Fig.3.**

105

106 **Supplementary Note 3 | Comparison of GaN and TiO_2 for GaN/InP heterostructure**

107 **Supplementary Fig. 4** presents a systematic core-level XPS analysis of the GaN/InP
108 heterostructure at different stages of interface formation, ranging from bare InP, i.e., before (gray)
109 and after (red) wet-chemical etching using 1M HCl (aq), to progressively thicker GaN overlayers.
110 The comparison between bare InP before and after wet-chemical etching provides a reference point
111 for separating contributions of native oxides from interface-related species formed during GaN
112 growth. Before etching, the InP surface shows clear signatures of a chemically complex native
113 oxide, with oxide-hydroxide and phosphate-related components visible in the P 2p at BE of 132.5
114 eV-136 eV, the pronounced shoulder at higher BE in In $3d_{5/2}$, and O 1s spectra. In the fitting of the
115 In $3d_{5/2}$ spectrum, the emission at 444.5 eV is correlated with In−P as a bulk-like bond in InP,
116 whereas the emissions at 445.90 eV (orange) and at 445.6 eV (blue) are related to In−O−P and In-
117 OH/In-OOH bonds. Due to the strong overlap of In–O–In (In_2O_3-like) and In–P emission lines, a
118 reliable separation of these contributions is not feasible within the present spectral resolution;
119 potential presence cannot be excluded. The emission attributed to In−O−P is also observed in the
120 P 2p region at 132-136 eV, as illustrated in orange. After etching in 1 M HCl, these contributions
121 are strongly reduced, indicating effective removal of phosphate-rich surface oxides. However, a
122 closer look at higher BE of In $3d_{5/2}$ core level reveals weak residual features, which may be
123 associated with In–OH or In_2O_3 species, as well as traces of $InCl_x$ formed during the etching
124 process. Consistent with these observations, the O 1s spectra show features that support the

125 presence of In-O and In-OH bonds together with contributions associated with C–O–related bonds.
126 This residual oxide, therefore, represents the starting surface onto which GaN is deposited.

127 With increasing GaN thicknesses, the InP-related P 2p and In $3d_{5/2}$ signals progressively decrease
128 in intensity, consistent with gradual surface coverage by the GaN overlayer. At low GaN
129 thicknesses (1–3 nm), the spectra indicate a mixed interfacial chemistry.

130 In this regime, oxide-related components in the In $3d_{5/2}$ and P 2p regions coexist with emerging N
131 1s and Ga-2p signals. The O 1s spectra evolve significantly with increasing GaN thickness,
132 displaying changes in peak shape and binding energy that reflect a redistribution of oxygen
133 bonding configurations. Although no external oxygen source was introduced during ALD, the
134 detected interfacial oxygen species most likely originate from transformations of residual native
135 oxides into phosphate-like species during the first stages of GaN growth. At a few cycles of GaN
136 (within the first ~20 cycles), the surface may not yet be fully covered, leaving areas exposed to air
137 where oxygen can still create oxide/hydroxide bonds. This interpretation is supported by the In
138 $3d_{5/2}$ spectra, which show higher-binding-energy asymmetry attribute to In–OH/In–OOH, In–O_x
139 and $InPO_x$ species, as well as weak components at 445–445.7 eV range at GaN thicknesses of 3–
140 5 nm. At the same time, the P 2p higher-binding energy region exhibits an increase in intensity,
141 indicating the formation of oxidized and nitrogen-containing phosphorus species. Possible
142 assignments for these P 2p photoemission peaks include $InPO_x$, $GaPO_x$, and P–NO_x species.
143 However, the contribution of $InPO_x$ is expected to be limited, as no correspondingly strong PO_x-
144 related signal is observed in the In $3d_{5/2}$ region. In contrast, the presence of $GaPO_x$ is supported by
145 the Ga $2p_{3/2}$ spectra and the Ga 3d inset, where oxide- and phosphate-related Ga components are
146 resolved. In addition, the increase at higher binding energy in the P 2p region may partially
147 originate from P–O-N, P–N species and P–O–Ga bonds. These observations indicate that the early-
148 stage GaN/InP interface is not simply oxide-derived but evolves toward a nitride-containing
149 interfacial chemistry in which P–N-related species become predominant. Although residual
150 oxide/phosphate components remain detectable at very low GaN thickness, the deconvolution
151 indicates that P–N and related Ga–N–P linkages are substantially enriched, whereas any In–N
152 contribution is much smaller, amounting for only ~20% of the fitted P–N component. Thus, within
153 the sensitivity of the XPS measurements, the interfacial chemistry is P–N-dominated nitride
154 component with trace amount of residual oxides.

155

156 Supplementary Note 4 | Flat band potential of Pt/GaN/p-InP in ferricyanide/ferrocyanide 157 redox couple

158 As shown in **Supplementary Fig. 5**, in ferricyanide/ferrocyanide, the flat-band potential shifted
159 to 1.64 V vs NHE, reflecting the ~0.36 V difference in redox potential compared to in 1 M $HClO_4$
160 bubbled with 1 atm H_2. This redox-dependent alignment indicates that the GaN/InP forms a solid–
161 liquid junction in which the band edges of GaN-passivated InP shift together with the
162 electrochemical potential of the ferricyanide/ferrocyanide solution[4]. Importantly, the barrier height

163 for electrons of ~1.23 V is preserved in both H^+/H_2 and ferricyanide/ferrocyanide redox couple.
164 Therefore, these dynamic band edge positions at difference redox couple enables efficient charge-
165 carrier separation under diverse (photo-)electrochemical environments and accounting for the high
166 photocatalytic activity of GaN/InP.

167

168 **Reference**

169 1. Zare Pour MA, Qaisrani MN, Höhn C, Wolf JL, Mogharehabed N, Velazquez Rojas J*, et al.* Composition and
170 Resulting Band Alignment at the TiO_2/InP Heterointerface: A Fundamental Study Combining Photoemission
171 Spectroscopy and Theory. *Adv. Funct. Mater.*, **36**(21)**:** 2506105.
172 2. Lin Y, Kapadia R, Yang J, Zheng M, Chen K, Hettick M*, et al.* Role of TiO_2 Surface Passivation on Improving
173 the Performance of p-InP Photocathodes. *J. Phys. Chem. C* 2015, **119**(5)**:** 2308-2313.
174 3. Shen X, Zhao T, Su H, Yang M, Chen J, Liu Y*, et al.* Tuning Intermediate Bands of Protective Coatings to
175 Reach the Bulk-Recombination Limit of Stable Water-Oxidation GaP Photoanodes. *Adv. Energy Mater.* 2022,
176 **12**(29)**:** 2201314.
177 4. Mills TJ, Lin F, Boettcher SW. Theory and Simulations of Electrocatalyst-Coated Semiconductor Electrodes
178 for Solar Water Splitting. *Phys. Rev. Lett.* 2014, **112**(14)**:** 148304.

179